We are IntechOpen, the world's leading publisher of Open Access books Built by scientists, for scientists

4,800
Open access books available

122,000
International authors and editors

135M
Downloads

Our authors are among the

154
Countries delivered to

TOP 1%
most cited scientists

12.2%
Contributors from top 500 universities

CLARIVATE ANALYTICS BOOK CITATION INDEX INDEXED

WEB OF SCIENCE™

Selection of our books indexed in the Book Citation Index in Web of Science™ Core Collection (BKCI)

Interested in publishing with us?
Contact book.department@intechopen.com

Numbers displayed above are based on latest data collected.
For more information visit www.intechopen.com

Chapter 10

Liquid-Crystal-Based Phase Gratings and Beam Steerers for Terahertz Waves

Ci-Ling Pan, Chia-Jen Lin, Chan-Shan Yang, Wei-Ta Wu and Ru-Pin Pan

Additional information is available at the end of the chapter

http://dx.doi.org/10.5772/intechopen.70449

Abstract

We review our theoretical and experimental studies on a class of liquid crystal (LC) photonic devices, i.e., terahertz (THz) phase gratings and beam steerers by using LCs. Such gratings can function as a THz polarizer and tunable THz beam splitters. The beam splitting ratio of the zeroth-order diffraction to the first-order diffraction by the grating can be tuned from 10:1 to 3:5. Gratings with two different base dimensions were prepared. The insertion loss is lower by approximately 2.5 dB for the one with the smaller base. The response times of the gratings were also studied and were long (tens of seconds) as expected because of the thick LC layer used. Accordingly, the devices are not suitable for applications that require fast modulation. However, they are suitable for instrumentation or apparatuses that require precise control, e.g., an apparatus requiring a fixed beam splitting ratio with occasional fine tuning. Schemes for speeding up the device responses were proposed. Based on the grating structure, we also achieved an electrically tunable THz beam steerer. Broadband THz radiation can be steered by 8.5° with respect to the incident beam by varying the driving voltages to yield the designed phase gradient.

Keywords: liquid crystals, liquid crystal devices, diffraction, phase grating, grating arrays, polarizer, beam splitter, submillimeter wave, THz radiation, tunable circuits and devices, ultrafast optics, beam steering

1. Introduction

Terahertz (THz) science and technology have advanced significantly over the last 3 decades. Applications are abundant in topics such as material characterization, data communication, biomedicine, 3D imaging, and environmental surveillance [1–5]. These developments were hampered as crucial quasi-optic components such as phase shifters [6–9], phase gratings [10–12],

modulators [13, 14], attenuators [15], polarizers [16, 17], and beam splitters [18–21] in the THz range are still relatively underdeveloped.

To control the properties of electromagnetic waves at all wavelengths, periodic structures such as gratings are frequently employed. In the THz frequency range, gratings with various periods have been used for tailoring few-cycle pulses [22]. Gratings have also been used as couplers and filters [23]. Tunable THz devices based on an optically and electrically controlled carrier concentration in quantum-well structures have been demonstrated. However, these devices have a limited range of tunability and must be operated at cryogenic temperatures far below room temperature [24–26]. The potential of gratings with liquid-crystal-enabled functionalities was recognized 2 decades ago [27]. Recently, the focus has been on various tunable THz devices, such as phase shifters, filters, and switches that are controlled electrically or magnetically, employing liquid crystals, primarily nematic liquid crystals (NLCs) [6–10, 15, 16, 18, 27–33]. Previously, we demonstrated a magnetically controlled phase grating for manipulating THz waves [10]. This is based on magnetic-field-induced birefringence of the NLCs employed [34]. Nonetheless, electrically controlled phase gratings are generally regarded as desirable for many applications. Therefore, we also proposed and demonstrated an electrically controlled phase grating involving NLCs for THz waves [11]. However, the theoretical analysis was not described in detail and the issue of insertion loss was not touched upon in the previous communication.

Besides, there is an urgent need for THz beam steering devices for scanning the THz beam over the surface of targets to get full topological and spectral information, a metamaterial-based beam steerer has been demonstrated and achieved a maximal deflection angle of 6° [35]. Other groups employed highly-doped semiconductors, such as Indium antimonide (InSb) [36] and GaAs [37], so that the propagation properties of surface plasmons mode in highly-doped semiconductor slits can be tailored by changing the carrier density there [36]. On the other hand, the development of a reconfigurable THz antenna [38], which can electrically steer the THz beam or vary the beam shapes, are useful for applications, such as adaptive wireless, satellite communication networks, and automobile radar systems. The use of LC to construct a phase array for beam steering in millimeter wave range has also been reported recently [39].

In this chapter, we report our comprehensive experimental studies on a phase grating for THz waves. In particular, we analyzed the insertion loss in such gratings and devised an approach for improving the loss by 2.5 dB over existing designs. Further, we demonstrated an electrically tunable phase shifter array to modulate the phase of THz beam. By applying different voltages on each part of the phase array, we can achieve a gradient in phase shift. Finally, it is shown that the incident THz wave can be steered toward a selected direction.

2. Theoretical and experimental methods

2.1. Operation principles of the phase grating

We designed a binary phase grating consisting of alternating sections of two materials (fused silica and LCs) with different refractive indices. **Figure 1** shows the schematic of a generic

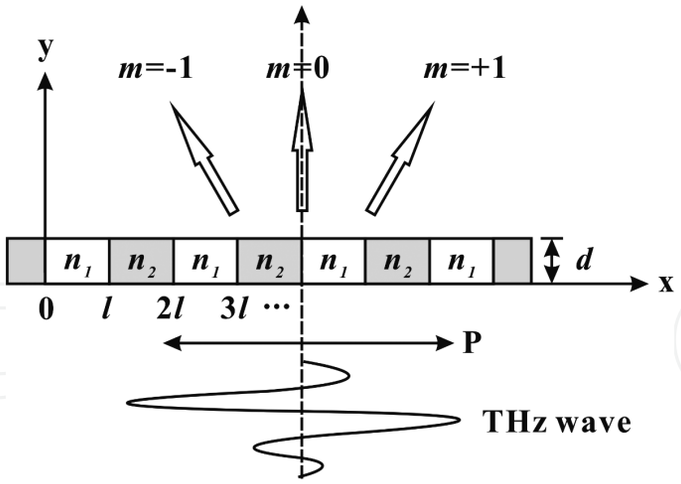

Figure 1. Schematic of a generic binary phase grating consisting alternating sections with refractive indices of n_1 and n_2. The width and height of each section of the phase element is respectively, l and d. P is the polarization direction of the THz wave.

binary phase grating. The grating is periodic along the x-direction. The THz wave is assumed to be polarized along the x-axis and propagates along the y-direction. Each section of the grating can be considered a retarder that introduces a phase shift. The Jones matrix [40] associated with a particular retarder can be written as

$$\widehat{R} = \begin{bmatrix} e^{i\delta_x} & 0 \\ 0 & e^{i\delta_y} \end{bmatrix}, \tag{1}$$

where δ is the phase retardation and a function of x. The Jones vector associated with the incident THz field is given by

$$E_i = E\begin{pmatrix} 1 \\ 0 \end{pmatrix}, \tag{2}$$

where E is a constant amplitude factor. The transmitted field E_t emerging from the retarder is then

$$E_t = \widehat{W} \cdot E_i = E\begin{pmatrix} e^{i\delta_x} \\ 0 \end{pmatrix}. \tag{3}$$

For our design, we set $\delta_x = n_N kd$, where $n_N = n_1 + \kappa_1$ or $n_2 + \kappa_2$ is the complex refractive index of the corresponding section, k is the wave number, and d is the thickness of the binary phase grating. The total transmitted field E_T is then the superposition of the field transmitted through all the alternating phase elements. We further write $E = E_0 e^{iky\sin\phi}$, where ϕ is the diffraction angle. Therefore, the total transmitted field can be written as

$$\begin{aligned} E_T(\varphi) = &\sum_{m=0}^{even} \int_{ml}^{(m+1)l} E_0 e^{iky\sin\varphi} e^{i(n_1+\kappa_1)kd} dy \\ &+ \sum_{m=1}^{odd} \int_{ml}^{(m+1)l} E_0 e^{iky\sin\varphi} e^{i(n_2+\kappa_2)kd} dy. \end{aligned} \tag{4}$$

In Eq. (4), l is the width of each section (all sections are assumed to have identical widths) of the grating. The diffraction intensity $I(\phi)$ can then be expressed as

$$I(\varphi) = E_T(\varphi) \cdot E_T^*(\varphi). \tag{5}$$

For an ideal binary phase grating, the diffraction efficiency η_m of the mth-order diffracted wave, defined as the intensity ratio of the diffracted beam to that of the incident beam, is given by

$$\eta_m = \frac{1}{\Lambda^2}\left|\int_{-\Lambda/2}^{\Lambda/2} e^{i\delta} e^{-i(2\pi m y/\Lambda)} dy\right|^2, \tag{6}$$

where δ is the x-dependent phase shift of the grating with grating period Λ [18, 41]. Following [41], we can write

$$\eta_m = \begin{cases} \cos^2(\Delta\Gamma/2) & \text{if } m = 0 \\ [(2/m\pi)\sin(m\pi/2)]^2 \sin^2(\Delta\Gamma/2) & \text{if } m \neq 0 \end{cases}, \tag{7}$$

where $\Delta\Gamma$ is the relative phase difference between two adjacent sections in the phase grating. For $\Delta\Gamma = (2N + 1)\pi$ (where N is an integer), the diffraction efficiencies of the odd orders ($m = \pm1, \pm3, \pm5, \ldots$) are maximal. Eq. (7) reveals that the diffraction efficiency of the third order $\eta_{\pm3}$ (4.5%) is nine times smaller than that of the first-order $\eta_{\pm1}$ (40.5%). Therefore, in this study, we considered only the zeroth and the first orders of the diffracted beam. Eqs. (6) and (7) were used as guides for designing the parameters of the grating. In practice, insertion loss causes the experimentally observed efficiencies to be lower than expected.

Because of the THz wavelength and THz beam size, the grating can have only a finite number of grooves. Further, the number of grooves N affects the angular resolution of the diffracted beam [42]. The angular width $\Delta\phi$ is given by

$$\Delta\varphi = \frac{\lambda}{N\Lambda\cos\varphi}. \tag{8}$$

Let the frequency of the THz be centered at 0.3 THz or a wavelength of 1 mm, we designed Λ to be 2 mm in our devices. The relative phase difference between adjacent sections is designed to be π. Therefore, the diffraction angle for the first order is 30°. **Figure 2** shows a plot of the diffraction efficiency as a function of the diffraction angle (for the first order). It illustrates clearly the angular resolution achievable for a grating with 10 periods and a grating with 40 periods. According to Eq. (8), the angular widths for the first-order diffracted wave for 10 and 40 periods are 3.3 and 0.8°, respectively.

When the relative phase difference between adjacent groves is tuned between π and 2π, the diffracted signals between the zeroth order and the first order have the maximal tunable range. This is illustrated in **Figure 3** for a grating with 10 periods. For $\Delta\Gamma = \pi$, the diffracted signal lies mainly in the first-order, and $\eta_{\pm1} \approx 0.4$. By contrast, for $\Delta\Gamma = 2\pi$, the diffracted signal mostly

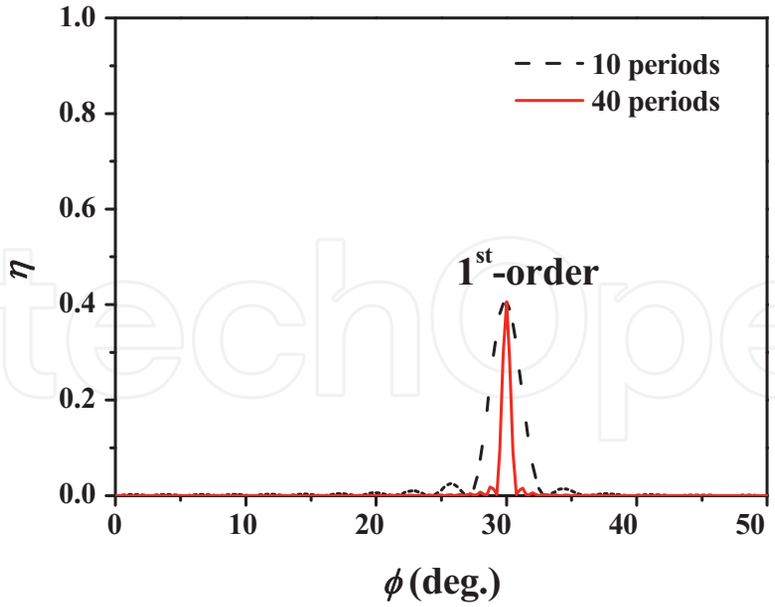

Figure 2. The diffraction efficiency of a phase grating with 10 (black dashed curve) and 40 periods (red solid line) is plotted as a function of the diffraction angle (for the first order).

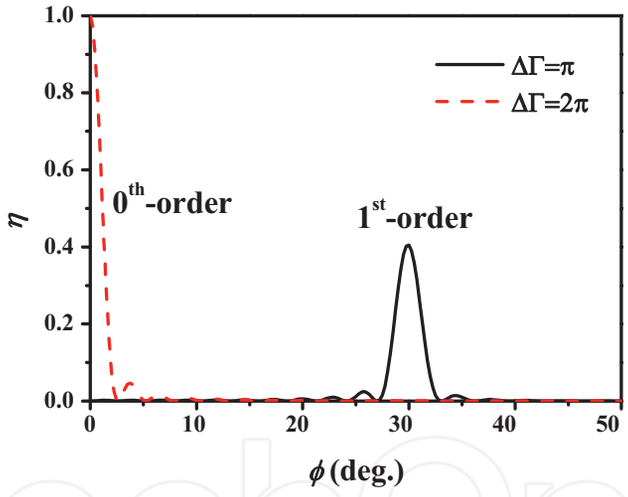

Figure 3. Diffraction efficiencies of a 10-period phase grating are plotted as a function of the diffraction angle for relative phase differences of π and 2π.

concentrated in the zeroth order, and $\eta_0 \approx 1$. These predictions are valid provided the insertion losses can be ignored.

2.2. Construction of the grating

The design of the grating was based on the structure of the electrically controlled THz phase grating reported in our previous study [11]. This is shown schematically in **Figure 4**. The incident THz wave was assumed to be polarized in the y-direction. Orientations of the LC molecules for two possible configurations are shown (See **Figure 4**). The device was designed

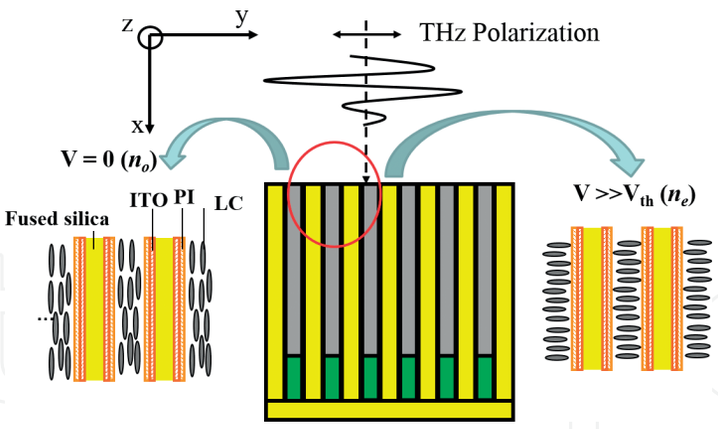

Figure 4. Structure of the electrically controlled THz phase grating using nematic liquid crystals. ITO: Indium tin oxide; PI: Polyimide; LC: Liquid crystal molecules; n_o: Ordinary index of refraction; n_e: Extraordinary index of refraction; V_{th}: Threshold voltage.

such that the frequency band of 0.3–0.5 THz would exhibit the highest zeroth-order diffraction efficiency.

Parallel grooves with a period of 2.0 mm, width of 1.0 mm, and groove depth of 2.5 mm were formed by stacking indium tin oxide (ITO)-coated fused silica substrates; the refractive index of these substrates is 1.95 in the sub-THz frequency region (0.2–0.8 THz). The surfaces of the fused silica substrates were coated with polyimide (SE-130B, Nissan) and then rubbed for homogenous alignment. The grooves were filled with NLCs (E7, Merck) and sealed with a sheet of fused silica coated with N,N-dimethyl-N-octadecyl-3-aminopropyltrimethoxysilyl chloride. At room temperature, E7 is a birefringent material with positive dielectric anisotropy. The LC molecules tend to be aligned parallel to the direction of the applied electric field when the applied voltage is greater than a threshold voltage. The effective refractive index of E7 [43], n_{eff} can be tuned from the refractive index for ordinary waves (n_o = 1.58) to that for extraordinary waves (n_e = 1.71) by varying the applied voltage. A stack of ITO-coated fused silica plates with dimensions identical to those of the grating was prepared as a reference. Bases of the phase grating with two different dimensions (h_1 = 17.5 mm and h_2 = 7.5 mm) were fabricated for analyzing the effect of dimension of the base on insertion losses of the phase grating.

2.3. Transmission measurements

A photoconductive (PC) antenna-based THz time-domain spectrometer (THz-TDS) [32, 44], was used for measuring the zeroth-order diffraction spectra of the device. Briefly, the pump beam from a femtosecond mode-locked Ti:sapphire laser was focused on a dipole antenna fabricated on LT-GaAs for generating a broadband THz signal, which was collimated and collected through the THz phase grating by using off-axis parabolic gold mirrors. A pair of parallel wire-grid polarizers (GS57204, Specac) was placed before and after the device under test. The zeroth-order diffraction of THz radiation was coherently detected by another PC antenna of the same type as that of the THz-TDS and grated by ultrafast pulses from the same laser.

In the second set of experiments, the broadband THz signal was filtered by using a metallic hole array to obtain a quasi-monochromatic wave centered at 0.3 THz and with a line width of 0.03 THz [45]. The diffraction pattern of this beam produced by a grating with various nematic LC orientations was detected and mapped by a liquid-helium-cooled Si bolometer, which was at a distance of 20 cm from the device and located on a rotating arm that could be swung with respect to the fixed grating. The bolometer had an aperture with a diameter of approximately 2.5 cm.

2.4. Insertion loss

To estimate the insertion loss of the THz grating, we regarded the device as a stack of parallel-plate waveguides. The ITO conductive film was not an ideal conductor. We recently showed that for a conductivity of 1500–2200 $\Omega^{-1}\cdot cm^{-1}$, the complex refractive indices of ITO are 20−70 for n and 20−70 for κ in the THz range [46]. On the basis of the manner of waveguide excitation, we can assume the mode of the propagating THz wave is transverse. The cutoff frequency of the parallel-plate waveguides can be written as $f_c = c/2\,nl$, where c is the velocity of light, l is the distance between two conductive layers, and n is the refractive index of the dielectric material within a waveguide. The attenuation constants α_c and α_d corresponding to conductor loss and dielectric loss, respectively, are given by [47, 48]

$$\alpha_c = \sqrt{\frac{\pi f \varepsilon}{\sigma_c}} \frac{2}{l\sqrt{(f_c/f)\left[1-(f_c/f)^2\right]}}, \tag{9}$$

and

$$\alpha_d = \frac{\pi f \tan\delta\sqrt{\varepsilon_r}}{c\sqrt{1-(f_c/f)^2}}, \tag{10}$$

where f is the frequency, ε is the permittivity of the dielectric material, σ_c is the conductivity of the electrode, tanδ is the loss tangent, and ε_r is the relative permittivity of the dielectric material. In practical applications, the insertion loss of the THz grating should be minimal.

2.5. Electrically controlled steering of the THz beam

We have also designed an electrically tunable phase shifter array which can function as the THz beam steerer. **Figure 5** shows the structure of the phase shifter array, which is constructed by alternately stacking a number of NLC layers and electrodes. Voltage sources are connected to the electrodes to apply control voltages to each NLC layer. The effective refractive index, n_{eff} (V), of each NLC layer can be electrically tuned by applying appropriate voltages. The polarization of the THz wave was assumed to be along the z-direction while the wave was normally incident to the device.

The device was designed such that, when no voltage was applied, the NLC molecules are aligned along the y-direction. In this case, the effective refractive index equals to that of the

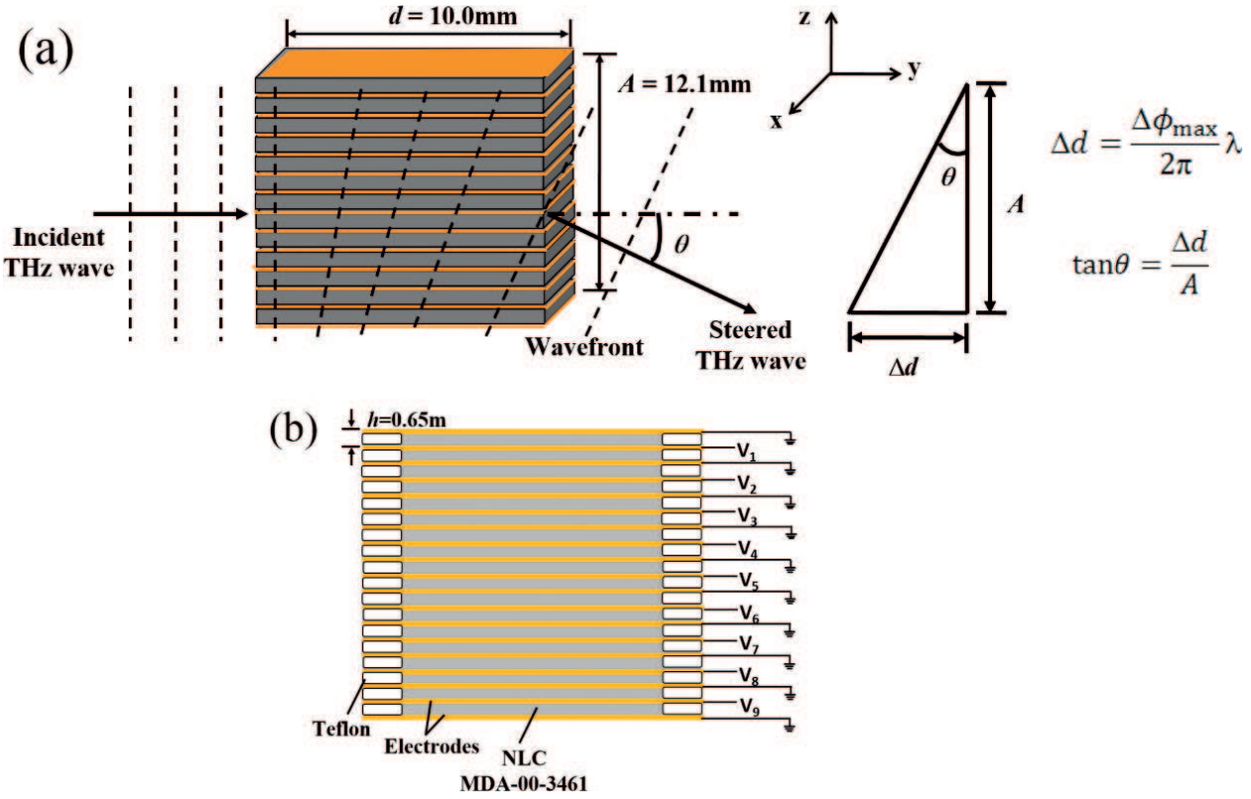

Figure 5. Schematic structure of the electrically controlled THz phase shifter array for beam steering. (a) Set-up of the beam steering experiment. The relationship between the steering angle, θ, optical delay length, Δd, and aperture, A, are shown. (b) Structure of the device with arrangement for voltage applied to each layer. Dimensions of the structure are also shown.

ordinary component of light in the LC, n_o. If sufficient control voltage is applied, the NLC molecules will orientate toward the direction parallel to the polarization direction of the THz wave (z-direction). The effective refractive index then equals to that of the extraordinary component of light in the LC, n_e. The traversing time, which the THz wave takes to pass through the NLC layers, can be changed by applying voltages. The corresponding phase shift $\Delta\phi(V)$ in the applying voltage V is given by

$$\Delta\phi(V) = kd\left(n_o - n_{eff}(V)\right), \tag{11}$$

where k is the wave number in free space and d is the propagation length of the NLC layer. When a certain phase gradient was created across the aperture of the device by adjusting the phase shift in each NLC layer, the wavefront of the transmitted wave was inclined against the aperture. According to the limited voltage source channels, we divided two NLC layers as a block. The steering angle θ can be determined by the aperture size A and the optical length delay Δd between the top NLC block and the bottom NLC block. The optical length delay Δd was according to the phase shift between the top and bottom NLC blocks $\Delta\phi_{\max}$. Therefore, the relationship between steering angle θ, optical length delay Δd, and the phase shift $\Delta\phi_{\max}$, was shown in **Figure 5(a)**, and can be written as,

$$\Delta d = \frac{\Delta\phi_{\max}}{2\pi}\lambda, \text{ and } \tan\theta = \frac{\Delta d}{A}, \tag{12}$$

where λ is the corresponding wavelength of THz wave. Accordingly, the THz wave can be steered by the control voltage. The phase shift $\Delta\phi_i$ in the certain ith NLC block, in our case can be written as,

$$\Delta\phi_i = (i-1)k(2h)\tan\theta, \tag{13}$$

where $2h$ was the thickness of the ith NLC block and θ was the steering angle against the normal of the aperture. We can see the construction of the device in **Figure 5(b)**, in which each NLC block includes two NLC layers and two electrodes.

In this work, we used the 550-μm-thick Teflon sheet as the spacer and the 100-μm-thick copper foil as the electrode. The copper foil was coated with PI Nissan SE-130B on both sides and rubbed for homogeneous alignment along y-direction before applying the voltage. The 18 NLC layers and 19 electrodes were stacked up alternately. The total thickness of the device was 12.1 mm, which corresponded to the size of the aperture, A, along z-direction. The size of the aperture along x-direction was designed to be 20.0 mm, and the propagation length, d, of the THz wave was designed to be 10.0 mm. Control voltage sources connected to the electrodes provided 1 kHz-sinusoidal waves to the NLC layers.

The threshold voltage V_c can be estimated by $V_c = \pi\ (k/\varepsilon_0\Delta\varepsilon)^{1/2} = 1.20\ V_{rms}$. The complex refractive indices of NLC MDA-00-3461 for ordinary and extraordinary in THz range are $n_o = 1.54$, $n_e = 1.72$, $\kappa_o = 0.03$, and $\kappa_e = 0.01$, respectively [49]. At a frequency of 0.3 THz, the

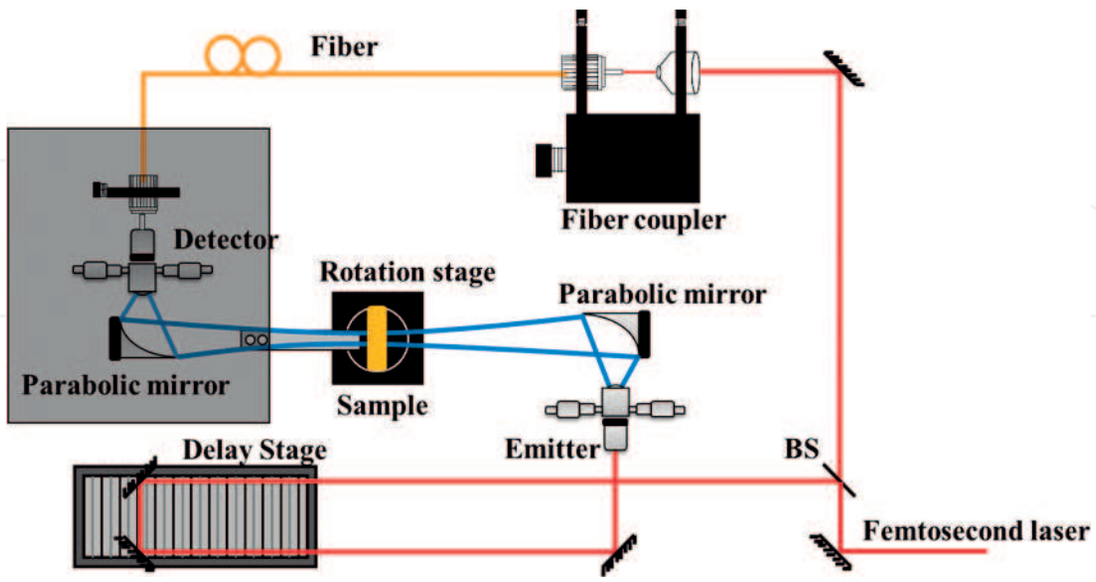

Figure 6. Improved THz-TDS. Probe beam is guided with a 1 m long optical fiber directly to the antenna. The detection assembly is located on a rotatable arm and can be moved without changing the optical path.

estimated maximum phase shift applied to a propagation wave passing through NLC layer would be 11.31 rad, which is calculated by Eq. (11) and the refractive indices of NLC MDA-00-3461. The maximum steering angle was estimated to be approximately 9° from Eq. (13) taking the maximum phase shift and aperture size into account.

For studying THz beam steering, we modified the THz-TDS by employing a 1 m-long single mode fiber (F-SF-C-1FC, from Newport Corp.) to guide the femtosecond laser directly to the detecting antenna. This way, the optical path remained fixed when the detecting arm was moved as the THz beam was steered. The schematic diagram of the setup is shown in **Figure 6**. The detection assembly was 20 cm away from the device and located on a rotation arm that can be swung with respect to the fixed device. This system was much more stable and convenient to use than the one employing the bolometer.

3. Results and discussions

3.1. Phase grating

We studied zeroth-order diffracted THz pulses by the phase grating for both ordinary and extraordinary waves were described in Ref. [11].

Experimentally, the diffraction efficiency of diffracted signals, η, in the frequency domain was determined by normalizing the diffracted signals in the frequency domain to the diffracted signals of the reference phase grating. To compare, a finite-difference time-domain (FDTD) algorithm (RSoft Design Group, Inc.) was used for simulating the diffraction of THz waves by a phase grating.

In the FDTD simulation, we analyzed the grating structure as a stack of rectangular-shaped waveguides. Neglecting conductive and magnetic loss of the materials involved, the Maxwell-Faraday and Maxwell-Ampere equations can be expanded in the Cartesian coordinates as

$$\begin{aligned}\frac{\partial H_x}{\partial t} &= \frac{1}{\mu_0}\left(\frac{\partial E_y}{\partial z} - \frac{\partial E_z}{\partial y}\right),\\ \frac{\partial H_y}{\partial t} &= \frac{1}{\mu_0}\left(\frac{\partial E_z}{\partial x} - \frac{\partial E_x}{\partial z}\right),\\ \frac{\partial H_z}{\partial t} &= \frac{1}{\mu_0}\left(\frac{\partial E_x}{\partial y} - \frac{\partial E_y}{\partial x}\right),\end{aligned} \tag{14}$$

$$\begin{aligned}\frac{\partial E_x}{\partial t} &= \frac{1}{\varepsilon_0}\left(\frac{\partial H_z}{\partial y} - \frac{\partial H_y}{\partial z}\right),\\ \frac{\partial E_y}{\partial t} &= \frac{1}{\varepsilon_0}\left(\frac{\partial H_x}{\partial z} - \frac{\partial H_z}{\partial x}\right),\\ \frac{\partial E_z}{\partial t} &= \frac{1}{\varepsilon_0}\left(\frac{\partial H_y}{\partial x} - \frac{\partial H_x}{\partial y}\right),\end{aligned} \tag{15}$$

where H_x, H_y, H_z, E_x, E_y, and E_z are components of the magnetic field and electric field, respectively. We set the refractive indices of the waveguides as those of fused silica and LCs.

http://dx.doi.org/10.5772/intechopen.70449

The two types of waveguides were made to alternate (black and yellow sections in **Figure 4**) in the structure. The grating device extended from $z = 0$ to $z = 2500$ μm. The incident wave was set to have a Gaussian shape, and the beam size was 19.0 mm, as large as the device aperture. The wave was normally incident in the z-direction from a source at $z < 0$ and was polarized in the x-direction. The dimensions of the grid in the FTD analysis were 10 μm × 10 μm in the xy-plane, while the time step was 1.67×10^{-14} s. **Figure 7** shows the simulation results for an incident THz wave that is yet to enter the device (a), THz waves at two positions in the grating (b and c), and a THz wave that has emerged from the grating. The false color (in 256 levels) indicates the strength of the electric field at a given spatial point. In **Figure 7(b, c)**, we show THz waves transmitted through the grating with different velocities at different x-positions because of the difference in the refractive indices. After the THz signal emerged from the device (**Figure 7(d)**), we set the time monitor to obtain the superposition signal.

To illustrate performance of the grating, experimental and FDTD simulation results of the zeroth-order diffraction efficiencies of the phase grating operated at four values of applied voltage are plotted as a function of frequency in **Figure 8** (reproduced from [11] with permission). Note that the experimentally measured diffraction efficiency was the highest near 0.3 THz, in agreement with the designed frequency. For an ordinary wave at 0.3 THz, the phase difference between fused silica and E7 was close to 2π. Therefore, the transmission of the

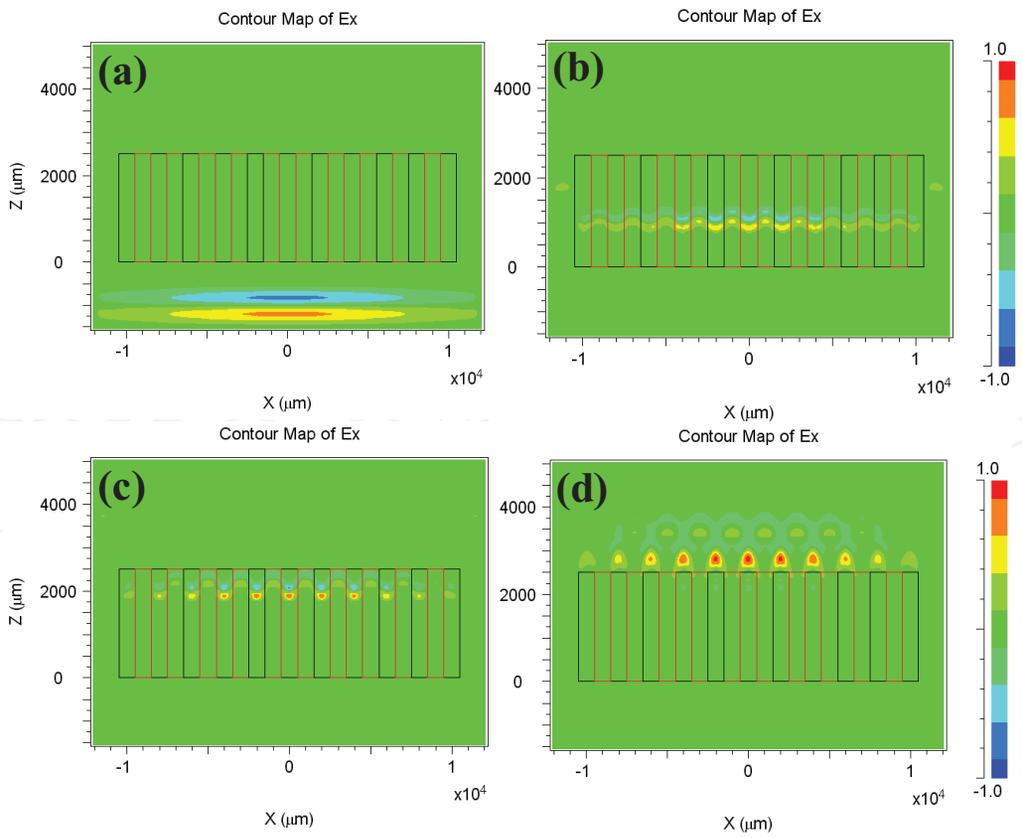

Figure 7. Simulation results for (a) an incident THz wave that is yet to enter the device, (b) and (c) THz waves at two positions in the grating, and (d) a THz wave that has emerged from the grating.

grating was higher. The THz wave was mainly concentrated in the zeroth order. By contrast, for extraordinary waves, the phase difference was close to π. Furthermore, the diffraction efficiency was lower for the zeroth order because the THz wave was mostly diffracted into the first order.

The experimental and FDTD simulation results are in general agreement. In **Figure 8(a, b)**, there are, however, some discrepancies in efficiencies and peak positions. This is expected as the thickness of the fused silica plates in the grating assembly varies by ±0.1 mm. To check, we calculated diffraction efficiencies of gratings with dimensions of 2.4, 2.5, and 2.6 mm using the

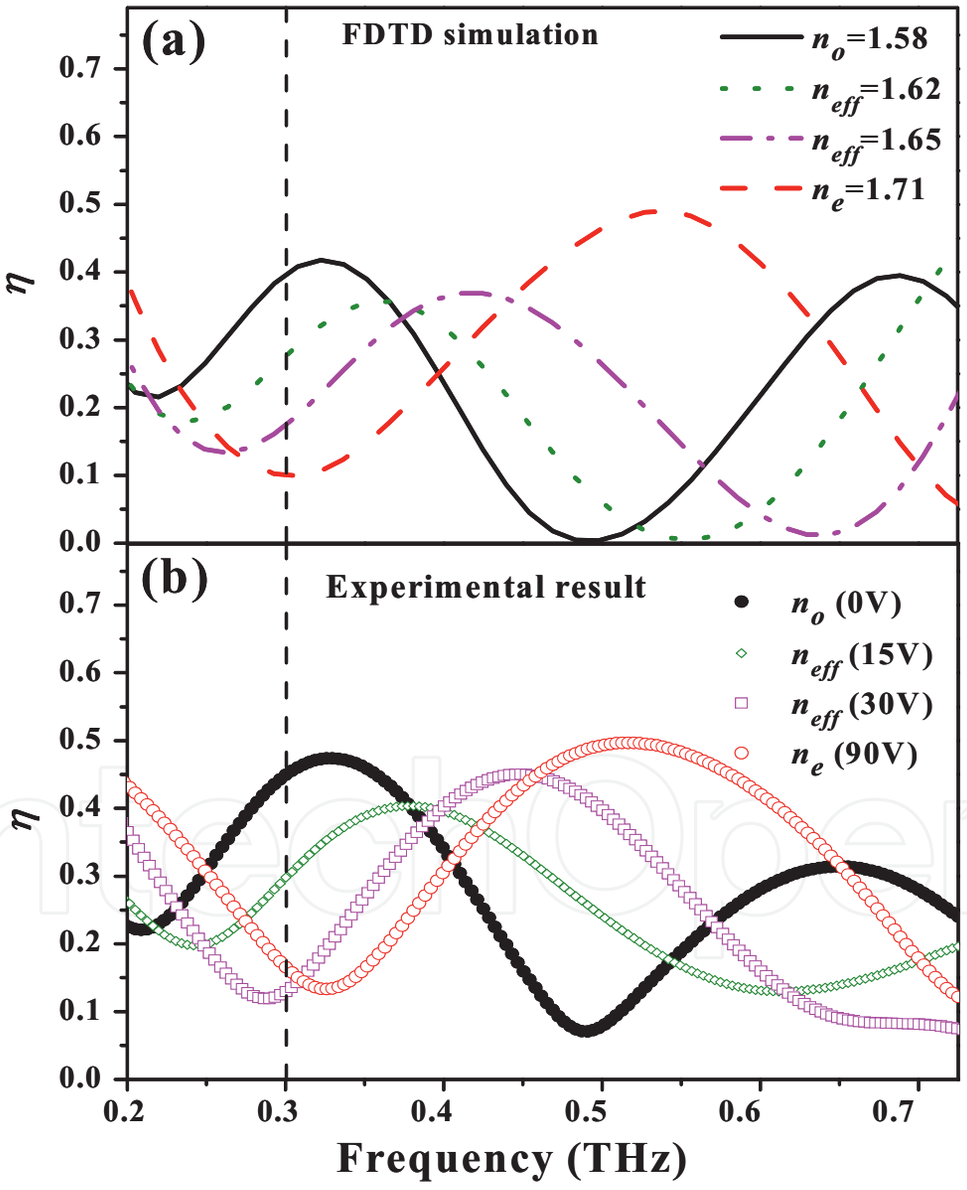

Figure 8. (a) FDTD simulation and (b) experimental results of the frequency dependence of the zeroth-order diffraction efficiencies of the phase grating operated at four values of applied voltages. (**Figure 3** of Ref. [11], reproduced by permission of the authors and IEEE).

http://dx.doi.org/10.5772/intechopen.70449

FDTD software for the o-ray and e-ray, respectively. Further, a structure with random arrangement of sections with deviations of 0.1 mm centered around 2.5 mm was also studied. The results are shown in **Figure 9**. Clear shifts are observed in the curves. Therefore, we inferred that the experimental results are reliable.

Because of the periodically arranged ITO films in the grating, our device could be considered a wire-grid polarizer for the THz wave. Only a THz wave polarized perpendicular to the grooves could pass through the electrically tuned phase grating. The measurement result is shown in **Figure 10**. The extinction ratio of the device shows the ratio of the transmitted THz signals polarized parallel and perpendicular to the grooves is better than 1:100 at ~ 0.3 THz.

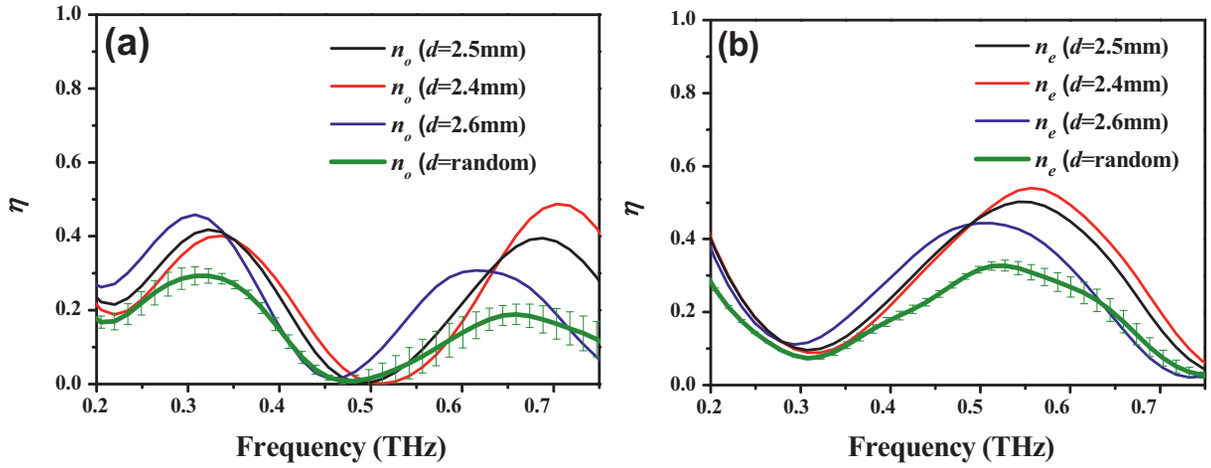

Figure 9. FDTD simulation result showing the diffraction efficiency as a function of the frequency for the phase grating of different thicknesses (see text): (a) o-wave and (b) e-wave.

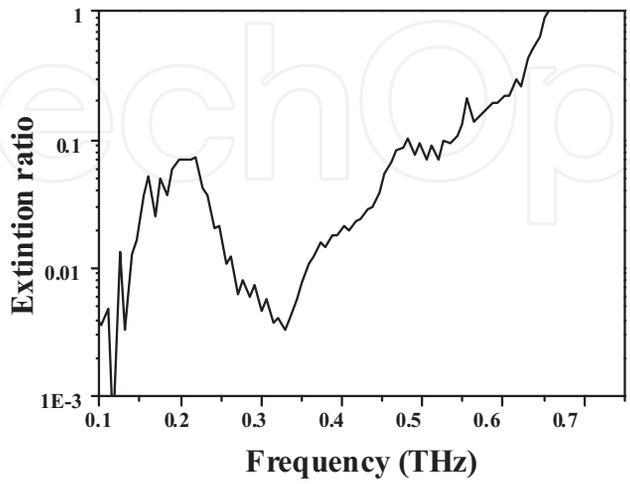

Figure 10. Extinction ratio of a sample. The data curve shows the proportion of THz-polarized transmitted signals parallel and perpendicular to the grooves.

3.2. Bolometer measurement results

In **Figure 11**, we present the intensity profiles of the diffracted 0.3 THz beam polarized in the y-direction. Data are shown for the grating biased from 0 to 90 V. The corresponding effective indices of refraction vary from 1.58 to 1.71. A diffraction maximum was detected at ϕ = 30°, which corresponds to the first-order diffracted beam predicted by the grating equation $\Lambda \sin\phi = m\lambda$, where Λ is 2.0 mm and the wavelength λ is 1.0 mm for the 0.3 THz wave. The measured diffraction efficiencies for the zeroth and first orders are in accord with the predictions of Eq. (5), considering the finite dimensions of the grating and the acceptance angle of the bolometer (±3°).

When the E7 molecules were aligned such that the refractive index was n_o, the phase difference was close to 2π. Most of the THz signal propagated in the direction of the zeroth-order diffraction. Experimentally, the diffraction efficiencies were determined to be 0.62 and 0.06 for the zeroth and first orders, respectively. The diffraction efficiencies were tuned by increasing the applied voltage (V_{appl}) gradually. When the refractive index of E7 was varied from 1.58 to 1.71, the diffraction efficiency of the zeroth order decreased; by contrast, the diffraction efficiency of the first order increased. When the E7 molecules were aligned such that the refractive index was n_e, the phase difference was close to π. The THz wave propagated mostly as a first-order diffracted beam. The diffraction efficiencies were 0.16 and 0.26 for the zeroth and first orders, respectively.

Figure 12(a, b) show the diffraction efficiencies of the zeroth and first orders as a function of the refractive index of E7 and V_{appl}. The experimental results, shown by dot symbols, are in good agreement with the theoretical predictions. Such results indicate that the grating functions as a variable beam splitter. The beam splitting ratio of the zeroth order to the first order can be tuned by varying the applied voltage.

Alternatively, these results indicate that the beam splitting ratio can be tuned and varied as a function of the refractive index of the nematic liquid crystal, E7. This is illustrated in **Figure 13**.

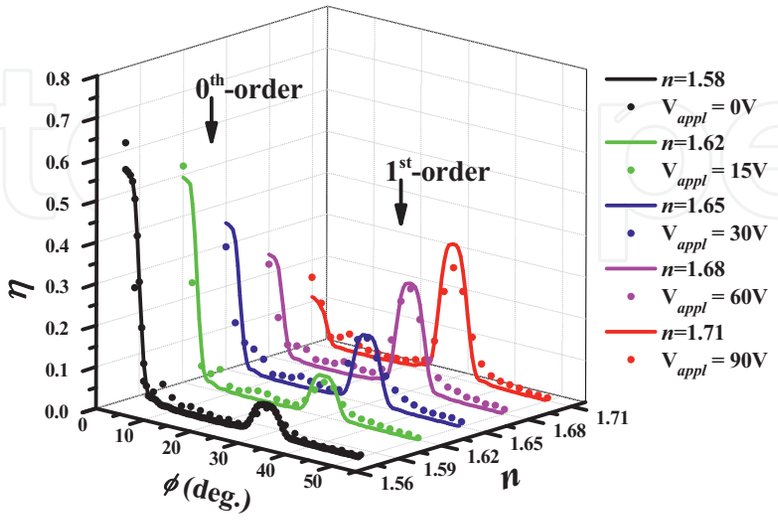

Figure 11. Diffraction efficiencies of the grating biased at several values of applied voltages are plotted as a function of the diffraction angle for the 0.3 THz beam. Solid lines are theoretical curves.

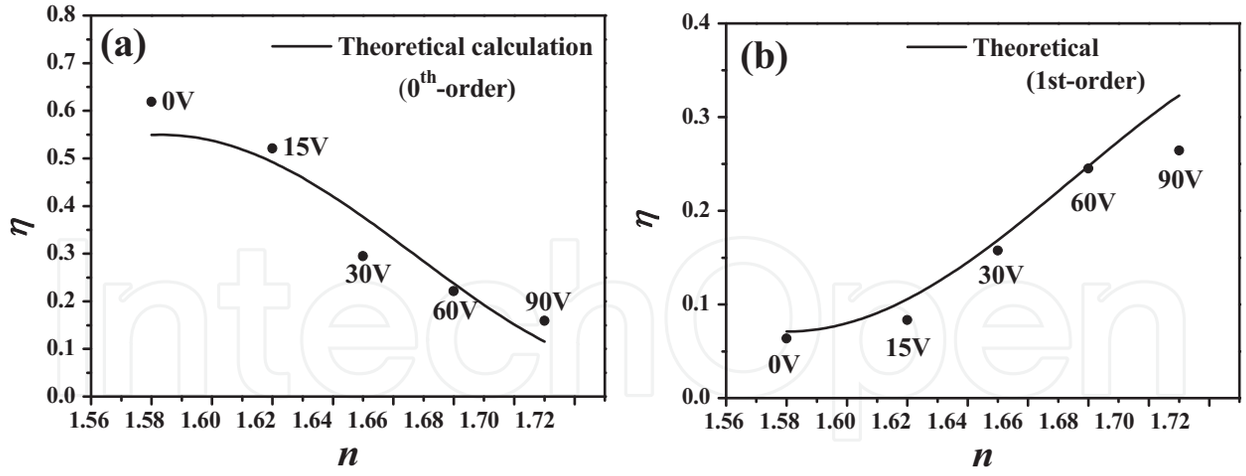

Figure 12. Diffraction efficiency as a function of the refractive index of E7 and the applied voltage for the (a) zeroth order and (b) first order. The theoretical calculation results and experimental results are shown by the curves and dots, respectively.

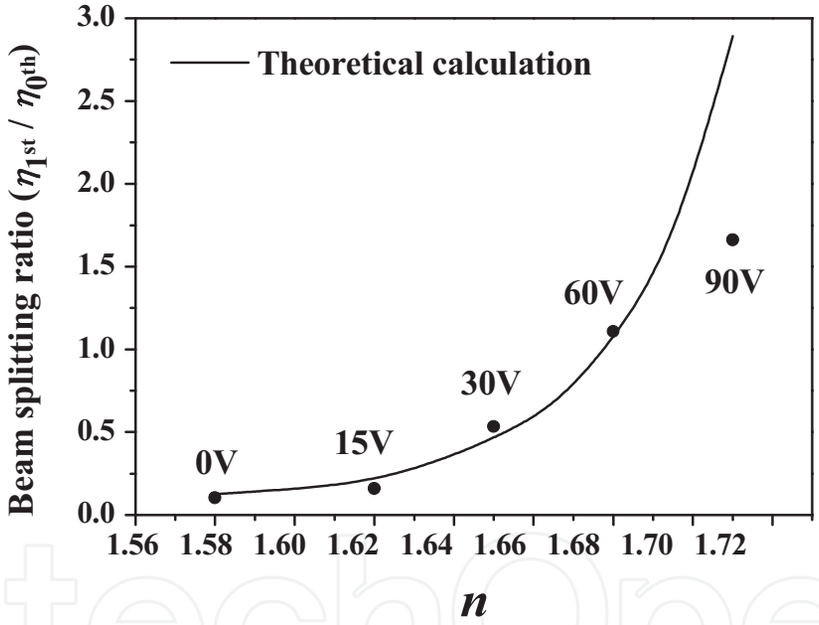

Figure 13. Beam splitting ratio as a function of the refractive index of E7. The theoretical calculation results and experimental results are shown by the curve and dots, respectively.

The theoretical calculation results and the experimental results are shown by the curve and dot symbols, respectively in **Figure 13**. The results indicate that the beam splitting ratio of the zeroth order to the first order can be tuned from 10:1 to 3:5.

3.3. Insertion loss

Insertion loss is a critical parameter for THz devices. We have experimentally and theoretically studied the insertion loss of two classes of devices. **Figure 14(a)** shows the diffraction efficiency

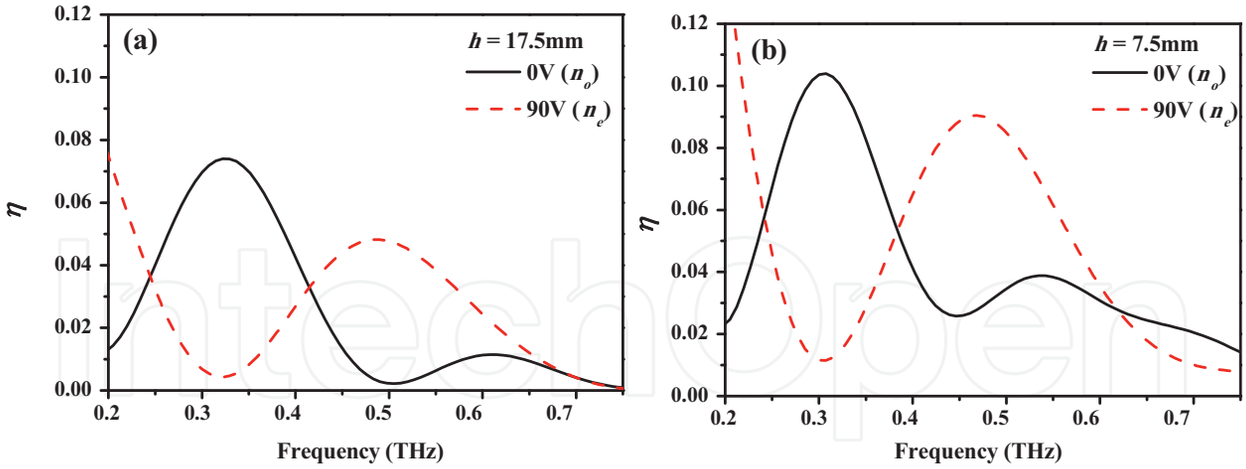

Figure 14. Diffraction efficiency of the devices with bases of (a) h = 17.5 mm and (b) h = 7.5 mm.

of a grating with a thicker base (h = 17.5 mm), obtained by normalizing the diffracted signals for the o-ray and e-ray to the reference THz signal for which the grating was removed. The experimentally measured diffraction efficiency for the o-ray at 0.3 THz is approximately 0.07. The diffraction efficiency for the o-ray at 0.3 THz predicted by the classic diffraction theory or evaluated by performing an FDTD simulation was approximately 0.45. The loss of the device was thus −8.0 dB for the o-ray at 0.3 THz. Similarly, the diffraction efficiency for the e-ray at 0.5 THz was approximately 0.046, whereas the theoretical prediction was approximately 0.45. The loss value of the grating for the e-ray at 0.5 THz was therefore −10 dB. A grating device with a smaller base component (h = 7.5 mm) was prepared to compare the insertion loss (**Figure 14(b)**). The experimentally measured diffraction efficiency for the o-ray at 0.3 THz was approximately 0.11, and the loss was −6.1 dB. The diffraction efficiency for the e−ray at 0.5 THz was approximately 0.083 and the loss value was −7.4 dB. The diffraction efficiency of the device with a smaller base is obviously higher than that of the device with a larger base.

The thickness of the ITO film we used was approximately 200 nm. According to [46], the conductivity σ of the film was $1.5 \times 10^3\ \Omega^{-1}\cdot cm^{-1}$. The parameters of fused silica and LC with different refractive indices in the frequency range of 0.2−0.8 THz are used for the insertion loss calculations shown in **Table 1**.

The estimated loss value was obtained from Eqs. (9) and (10). For the grating with a larger base component (h = 17.5 mm), the total loss for the o-wave at 0.3 THz and for the e-wave at 0.5 THz were estimated to be −9.0 and −13 dB, respectively. Similarly, for the grating with a smaller base component (h = 7.5 mm), the total loss for the o-wave at 0.3 THz and for the e-wave at

Material	Fused silica	E7 (n_o)	E7 (n_e)
ε_r	3.80	2.50	2.92
ε_i	0.008	0.095	0.041
tanδ	0.0021	0.038	0.014

Table 1. Parameters of fused silica and the NLC E7.

Phase grating	h = 17.5 mm		h = 7.5 mm	
Driving voltage	**0 V (n_o) at 0.3 THz**	**90 V (n_e) at 0.5 THz**	**0 V (n_o) at 0.3 THz**	**90 V (n_e) at 0.5 THz**
(Estimated insertion loss)				
Conductor loss	4.7 dB	7.8 dB	2.3 dB	3.8 dB
Dielectric loss	4.3 dB	4.9 dB	3.2 dB	3.1 dB
Total	9.0 dB	13 dB	5.5 dB	6.9 dB
Measured value	8.0 dB	10 dB	6.1 dB	7.4 dB

Table 2. Insertion loss of phase gratings.

0.5 THz were estimated to be −5.5 and −6.9 dB, respectively. **Table 2** shows the estimated and measured values of the two devices. The discrepancy between the estimated insertion loss and measured data could be due to the finite collection efficiency of the detection system and nonideal assembly of the grating. The experimental results indicate that by reducing the thickness of the thick fused silica plates in the base of the device by10 mm, the insertion loss can be reduced by approximately 2.5 dB.

Therefore, if a grating device without a base (h = 2.5 mm) can be fabricated, the insertion loss can be as low as −2.5 dB. Such a device would be more attractive for practical use. Furthermore, the performance of the grating can be improved by using electrodes with higher conductivity. The thickness of the electrodes affects the conductor loss, as detailed in Ref. [50].

3.4. Device response times

For gratings using LCs, the response time of the device is a concern. The voltage-on and voltage-off times were measured by subjecting the device to a pulse signal. **Figure 15(a, b)** shows the normalized power as a function of the driving voltage in the voltage-on and voltage-off states, respectively. We defined the rise time as the duration for which the driving voltage was turned on for reducing the power to 37% of the maximum. The fall time was defined as the duration for which the driving voltage was turned off for increasing the power

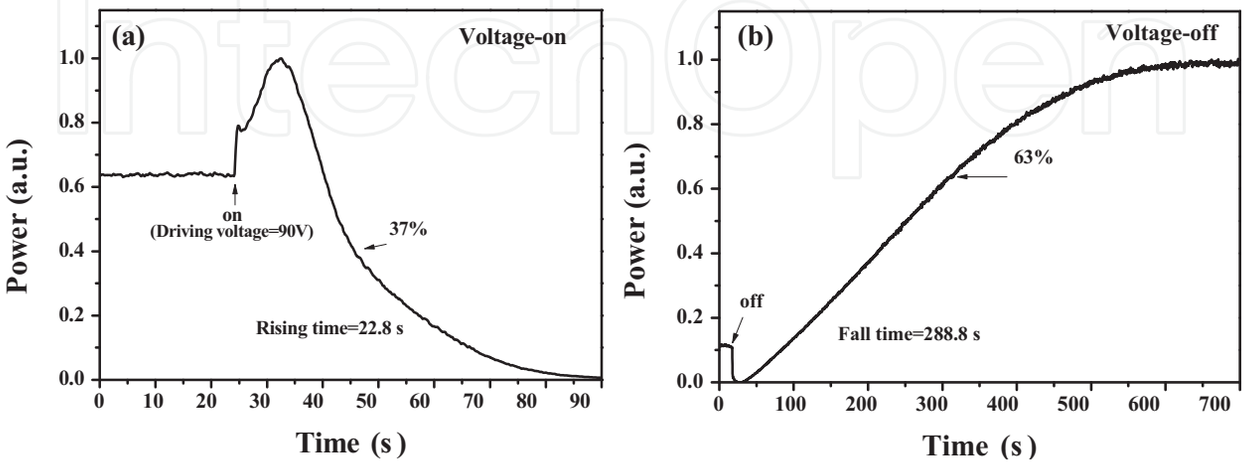

Figure 15. Response times of a phase grating: (a) voltage-on state and (b) voltage-off state.

to 63% of the maximum. The rise and fall times of the grating were found to be approximately 23 and 290 s, respectively. The phase grating responded slowly because of the thick LC layer used. Consequently, the present device is not suitable for applications that require fast modulation. However, the device is appropriate for instrumentation or apparatuses that require, for example, a fixed beam splitting ratio with occasional fine tuning.

The response time of the voltage-off state depended only on the material properties and cell thickness. Therefore, it cannot be shortened by applying a higher electric field. To shorten the response time, LCs with birefringence than E7 can be used. Alternatively, dual-frequency LCs can be employed; the use of dual-frequency LCs has been discussed in previous papers [51–54]. Dual-frequency LCs show high dielectric dispersion, and their dielectric anisotropy is frequency dependent, resulting in a change in sign at the crossover frequency. Dual-frequency materials in which the crossover frequency is a few kilohertz and changes markedly over the range are commercially available. Dual-frequency LCs would enable the operation of phase gratings in a nonzero applied voltage state.

3.5. Phase shifting and beam steering

We have studied the phase shift experienced by the THz wave propagating through the grating in which the control voltages were applied equally to all NLC layers. **Figure 16** shows the measured THz waveforms for biasing voltages varied from 0 to 28.8 V_{rms}. It is obviously that the pulses delay increase as applying voltages increased, as the NLC molecules re-orientate gradually from ordinary to extraordinary refractive index.

By applying Fourier transform on the waveforms in **Figure 16**, we obtained the phase shift as a function of frequency. This is shown in **Figure 17**. The phase shift increased with increasing

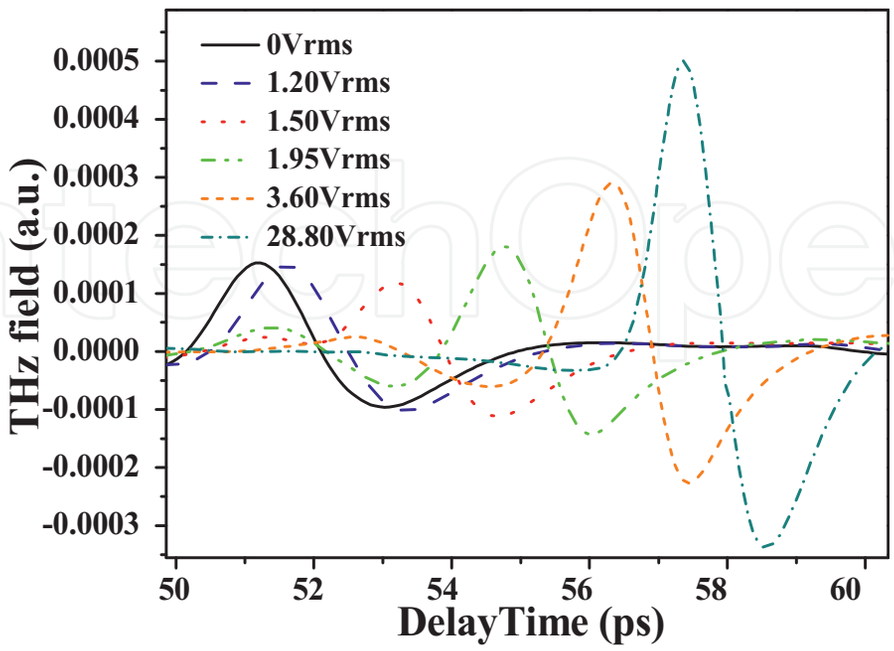

Figure 16. THz signal delay in time domain. Delay time increases as applying voltage increases.

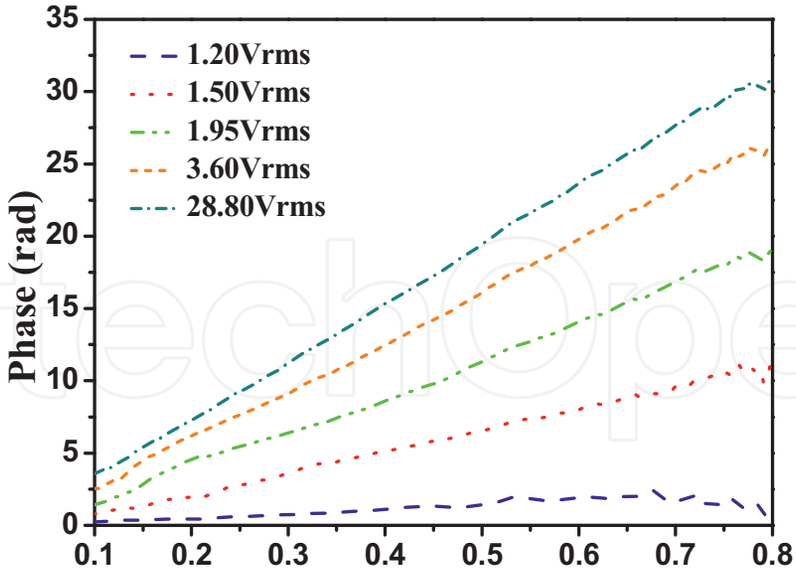

Figure 17. Spectra of phase shift of THz signal. Phase increases as applying voltage increases.

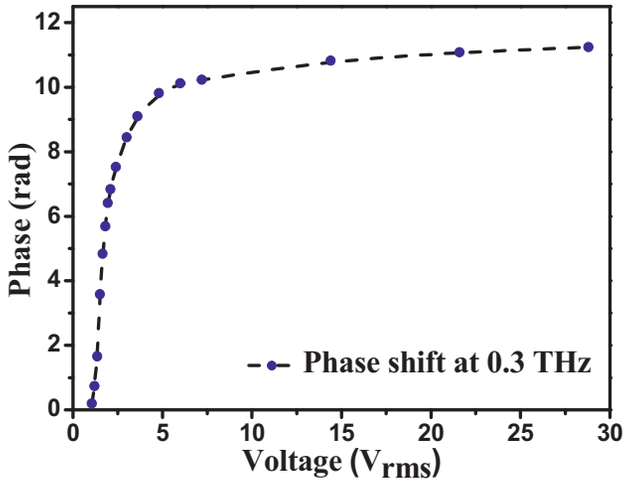

Figure 18. Phase shift at 0.3 THz as a function of the control voltage.

applying voltages as expected. **Figure 18** is a plot the phase shift at 0.3 THz as a function of the control voltage. Above the threshold voltage, 1.20 V_{rms}, the phase shift rapidly increases with the applying voltage. The maximum phase shift reached approximately 11.24 rad. This value is in close agreement with the calculated value.

We measured the beam steering characteristics of the phase-shifting array with the modified THz-TDS shown in **Figure 6**. Although the applying voltage should be adjusted layer-by layer for beam steering, only nine values of control voltages were available to be applied to each NLC block consisting two NLC layers. As the phase shift $\Delta\phi_i$ in each NLC block needed for beam steering is given by Eq. (12), the control voltage corresponding to phase shift can be determined from the experimental results in **Figure 18**, and are tabulated in **Table 3**.

	Applied voltage (V_{rms})	Phase shift (rad) at 0.3 THz
V_1	0	0
V_2	1.32	1.41
V_3	1.44	2.81
V_4	1.57	4.22
V_5	1.77	5.62
V_6	2.18	7.03
V_7	2.96	8.43
V_8	4.88	9.84
V_9	28.80	11.24

Table 3. Control voltage and corresponding phase shift at 0.3 THz.

The experimental results demonstrating beam steering are shown in **Figure 19**.

In the above figure, (a) shows the THz signal before transmitted to the device, and (b) and (c) show the THz signal transmitted through the device with ordinary and extraordinary refractive indices at $\theta = 0°$, respectively. The main beam was steered in the direction of $\theta = 8.5°$ as the control voltages were varied to yield the phase gradient as shown in (d). The signal vanishes as we removed the device as shown in (e). Applying FFT analysis, the corresponding THz spectra

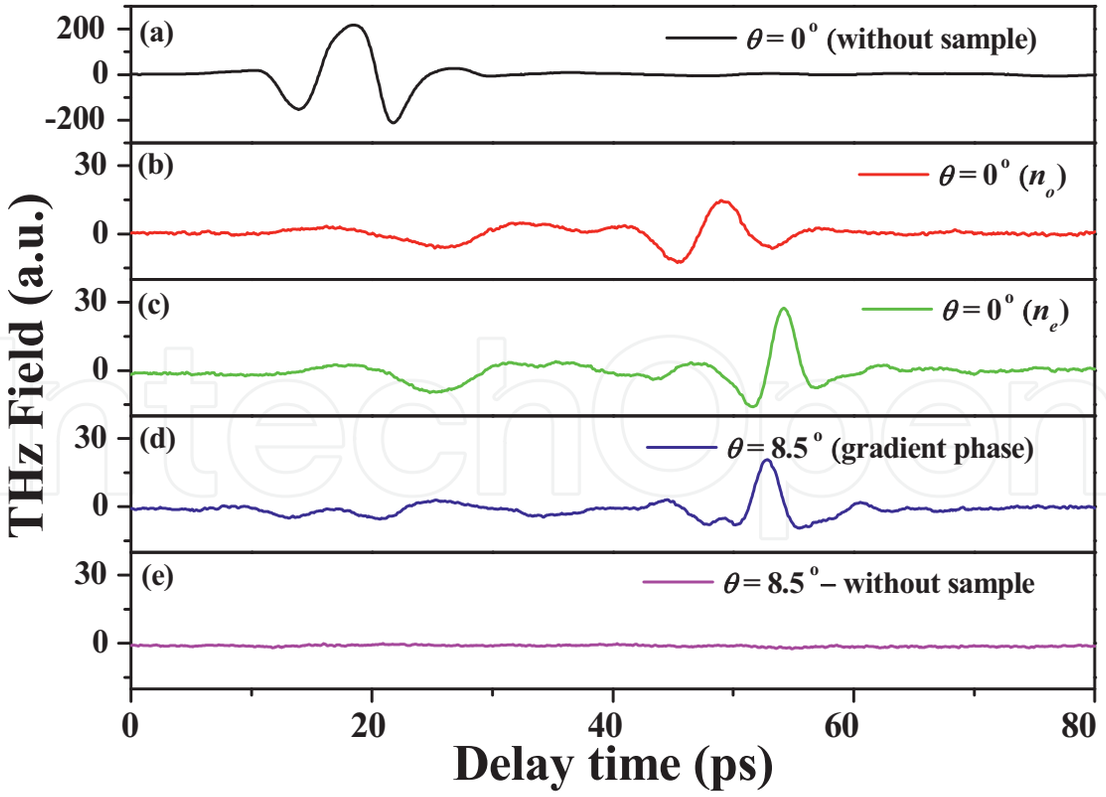

Figure 19. THz signals before steered at $\theta = 0°$: (a) without sample; with sample (b) at no-state, (c) at ne-state; steered signals at $\theta = 8.5°$: (d) sample applied voltage to yield gradient phase, (e) without sample.

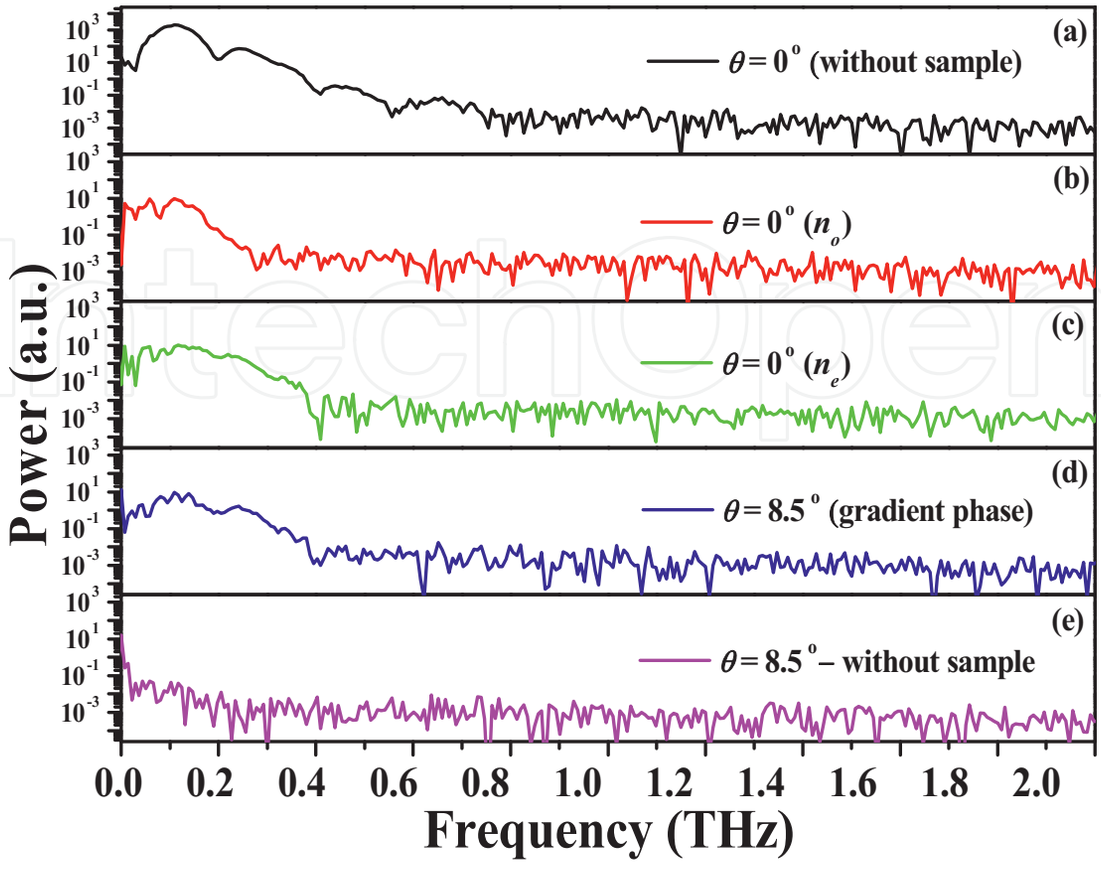

Figure 20. Spectra of THz signals before steered at $\theta = 0°$: (a) without sample; with sample (b) at no-state, (c) at ne-state; steered signals at $\theta = 8.5°$: (d) sample applied voltage to yield gradient phase, (e) without sample.

in frequency domain are shown in **Figure 20**. According to the results, the device can steer the broadband THz signal up to about 0.5 THz.

4. Summary

In this work, we review our theoretical and experimental studies on electrically controlled LC-based phase gratings for manipulating THz waves. This device can be used as a tunable THz beam splitter, and the beam splitting ratio of the zeroth-order diffraction to the first-order diffraction can be tuned from 10:1 to 3:5. An FDTD simulation was performed to investigate the diffraction effect of the phase grating. The experimental and simulation results were in general agreement. The signal losses of the device were discussed. It was observed that the insertion loss could be reduced by reducing the thickness of the fused silica plates in the base component of the device. The rise and fall times of the grating are approximately 23 and 290 s, respectively. The slow response could be accounted for because of the thick LC layer employed. Consequently, it is not suitable for applications that require fast modulation. However, the device is appropriate for instrumentation or apparatuses that require, for example, a fixed beam splitting ratio with occasional fine tuning. The use of highly-birefringent NLCs or dual-frequency LCs could alleviate the problem somewhat. Besides, we demonstrated a

grating-structured phase shifter array that can be used as the THz shifter and THz beam steerer. A phase shift as large as 11.24 rad was achieved. Using a designed voltage gradient biasing on the grating structure, broadband THz signal below 0.5 THz can be steered by as much as 8.5°. The experimental results are in good agreement with theoretical predictions.

Acknowledgements

This work was partly supported by the National Science Council of Taiwan (104–2221-E-007-093-MY3), the Academic Top University Program of the Taiwan Ministry of Education, and the U.S. Air Force Office of Scientific Research (FA2386–13–1-4086). Chia-Jen Lin is now with Taiwan Semiconductor Manufacturing Company. Contributions by Mr. Chuan-Hsien Lin are gratefully acknowledged.

Author details

Ci-Ling Pan[1]*, Chia-Jen Lin[2], Chan-Shan Yang[1], Wei-Ta Wu[2] and Ru-Pin Pan[2]

*Address all correspondence to: clpan@phys.nthu.edu.tw

1 Department of Physics, National Tsing Hua University, Hsinchu, Taiwan

2 Department of Electrophysics, National Chiao Tung University, Hsinchu, Taiwan

References

[1] Ferguson B, Zhang X-C. Materials for terahertz science and technology. Nature Materials. 2002;**1**:26-33

[2] Tonouchi M. Cutting-edge terahertz technology. Nature Photonics. 2007;**1**:97-105

[3] Zhang X-C, Xu J. Introduction to THz Wave Photonics. New York: Springer; 2010

[4] Nagatsuma T, Ducournau G, Renaud CC. Advances in terahertz communications accelerated by photonics. Nature Photonics. 2016;**10**:371-379

[5] Alonso-González P, Nikitin AY, Gao Y, Woessner A, Lundeberg MB, Principi A, Forcellini N, Yan W, Vélez S, Huber AJ, Watanabe K, Taniguchi T, Casanova F, Hueso LE, Polini M, Hone J, Koppens FHL, Hillenbrand R. Acoustic terahertz graphene plasmons revealed by photocurrent nanoscopy. Nature Nanotechnology. 2017;**12**:31-35

[6] Yang C-S, Tang T-T, Chen P-H, Pan R-P, Yu P, Pan C-L. Voltage-controlled liquid-crystal terahertz phase shifter with indium-tin-oxide nanowhiskers as transparent electrodes. Optics Letters. 2014;**39**(8):2511-2513

[7] Yang C-S, Tang T-T, Pan R-P, Yu P, Pan C-L. Liquid crystal terahertz phase shifter s with functional indium-tin-oxide nanostructures for biasing and alignment. Applied Physics Letters. 2014;**104**:141106

[8] Yang C-S, Kuo C, Tang C-C, Chen JC, Pan R-P, Pan C-L. Liquid-crystal terahertz quarter-wave plate using chemical-vapor-deposited graphene electrodes. IEEE Photonics Journal. 2015;**7**(6):2200808

[9] Pan CL, Pan RP, Yang CS, Yu P, Voltage-controlled 2 liquid-crystal terahertz phase shifter with indium-tin-oxide (ITO) nanowhiskers as transparent electrodes. In: The XXXI General Assembly of the International Union of Radio Science, paper DFC01.6, Beijing, China. Aug 16–13, 2014

[10] Lin C-J, Li Y-T, Hsieh C-F, Pan R-P, Pan C-L. Manipulating terahertz wave by a magnetically tunable liquid crystal phase grating. Optics Express. 2008;**16**:2995-3001

[11] Lin C-J, Lin C-H, Li Y-T, Pan R-P, Pan C-L. Electrically controlled liquid crystal phase grating for terahertz waves. IEEE Photonics Technology Letters. 2009;**21**:730-732

[12] Mirzaei B, Silva JRG, Luo YC, Liu XX, Wei L, Hayton DJ, Gao JR, Groppi C. Efficiency of multi-beam Fourier phase gratings at 1.4 THz. Optics Express. 2017;**25**:6581-6588

[13] Chen H-T, Padilla WJ, Cich MJ, Azad AK, Averitt RD, Taylor AJ. A metamaterial solid-state terahertz phase modulator. Nature Photonics. 2009;**3**:148-151

[14] Nouman MT, Kim H-W, Woo JM, Hwang JH, Kim D, Jang J-H. Terahertz modulator based on metamaterials integrated with metal-semiconductor-metal varactors. Scientific Reports. 2016;**6**:26452

[15] Wang M, Vajtai R, Ajayan PM, Kono J. Electrically tunable hot-silicon terahertz attenuator. Applied Physics Letters. 2014;**105**:141110

[16] Hsieh C-F, Lai Y-C, Pan R-P, Pan C-L. Polarizing terahertz waves with nematic liquid crystals. Optics Letters. 2008;**33**:1174-1176

[17] Farid A, Laurita NJ, Tehrani B, Hester JG, Tentzeris MM, Armitage NP. Inkjet printed wire-grid polarizers for the THz frequency range. Journal of Infrared, Millimeter and Terahertz Waves. 2017;**38**:276-282

[18] Park J-H, Yu C-J, Kim J, Chung S-Y, Lee S-D. Concept of a liquid-crystal polarization beamsplitter based on binary phase gratings. Applied Physics Letters. 2003;**83**: 1918-1920

[19] Berry CW, Jarrahi M. Broadband terahertz polarizing beam splitter on a polymer substrate. Journal of Infrared, Millimeter and Terahertz Waves. 2012;**33**:127-130

[20] Ung BS-Y, Fumeaux C, Lin H, Fischer BM, Ng BW-H, Abbott D. Low-cost ultra-thin broadband terahertz beam-splitter. Optics Express. 2012;**20**(5):4968-4978

[21] Mo G-Q, Li J-S. Compact terahertz wave polarization beam splitter using photonic crystal. Applied Optics. 2016;**55**:7093-7097

[22] Filin A, Stowe M, Kersting R. Time-domain differentiation of terahertz pulses. Optics Letters. 2001;**26**:2008-2010

[23] Garet F, Coutaz J–L, Narzarov M, Bonnet E, Parriaux O, Racine G, THz time-domain spectroscopy study of grating couplers and segmented grating filters. In: IEEE 2004 Joint 29th Int. Conf. on Infrared and Millimeter Waves and 12th Int. Conf. on Terahertz Electronics. Oct 2004. pp. 181-182

[24] Kersting R, Strasser G, Unterrainer K. Terahertz phase modulator. Electronics Letters. 2000;**36**:1156-1158

[25] Kleine-Ostmann T, Dawson P, Pierz K, Hein G, Koch M. Room-temperature operation of an electrically driven terahertz modulator. Applied Physics Letters. 2004;**84**:3555-3557

[26] Libon IH, Baumgärtner S, Hempel M, Hecker NE, Feldmann J, Koch M, Dawson P. An optically controllable terahertz filter. Applied Physics Letters. 2000;**76**:2821-2823

[27] Chen J, Bos PJ, Vithana H, Johnson DL. An electro-optically controlled liquid crystal diffraction grating. Applied Physics Letters. 1995;**67**:2588-2590

[28] Chen CY, Hsieh CF, Lin YF, Pan RP, Pan CL. Magnetically tunable room-temperature 2π liquid crystal terahertz phase shifter. Optics Express. 2004;12:2625-2630

[29] Wu HY, Hsieh CF, Tang TT, Pan RP, Pan CL. Electrically tunable room-temperature 2π liquid crystal terahertz phase shifter. IEEE Photonics Technology Letters. 2006;**18**:1488-1490

[30] Chen C-Y, Hsieh C-F, Lin Y-F, Pan C-L, Pan R-P. Liquid- crystal-based terahertz tunable Lyot filter. Applied Physics Letters. Mar. 2006;**88**:101107

[31] Ho I-C, Pan C-L, Hsieh C-F, Pan R-P. Liquid- crystal- based terahertz tunable Solc filter. Optics Letters. 2008;**33**:1401-1403

[32] Ghattan Z, Hasek T, Wilk R, Shahabadi M, Koch M. Sub- terahertz on–off switch based on a two-dimensional photonic crystal infiltrated by liquid crystals. Optics Communication. 2008;**281**:4623-4625

[33] Jewell1 SA, Hendry E, Isaac TH, Sambles JR. Tuneable Fabry–Perot etalon for terahertz radiation. New Journal of Physics. 2008;**10**:033012

[34] Pan R-P, Hsieh C-F, Chen C-Y, Pan C-L. Temperature- dependent optical constants and birefringence of nematic liquid crystal 5CB in the terahertz frequency range. Journal of Applied Physiology. 2008;**103**:093523

[35] Neu J, Beiggang R, Rahm M. Metamaterial-based gradient index beam steerers for terahertz radiation. Applied Physics Letters. 2013;**103**:041109

[36] Xu B, Hu H, Liu J, Wei X, Wang Q, Song G, Xu Y. Terahertz light deflection in doped semiconductor slit arrays. Optics Communication. 2013;**308**:74-77

[37] Xu Z, Mazumder P. Terahertz beam steering with doped GaAs phase modulator and a design of spatial-resolved high-speed terahertz analog-to-digital converter. IEEE Transactions on Electron Devices. 2014;**61**:2195-2202

[38] Bin Shams MI, Jiang Z, Qayyum J, Rahman S, Fay P, Liu L. A terahertz reconfigurable photo-induced fresnel-zone-plate antenna for dynamic two-dimensional beam steering and forming. In: Microwave Symposium (IMS), 2015 IEEE MTT-S International, Phonenix, AZ. May 2015. pp. 1-4

[39] Kamoda H, Kuki T, Fujikake H, Nomoto T. Millimeter-wave beam former using liquid crystal. In: Microwave Conference, 2004. 34th European, Amsterdam, The Netherlands. Oct 2004. pp. 1141-1144

[40] Brosseau C. Fundamentals of Polarized Light. New York: Wiley; 1998

[41] Goodman JW. Introduction to Fourier Optics. 2nd ed. McGraw-Hill; 1996

[42] Fowles JR. Introduction to Modern Optics. 2nd ed. Holt, Rinehart and Winston; 1975

[43] Yang C-S, Lin C-J, Pan R-P, Que CT, Yamamoto K, Tani M, Pan C-L. The complex refractive indices of the liquid crystal mixture E7 in the terahertz frequency range. Journal of the Optical Society of America B: Optical Physics. 2010;**27**:1866-1873

[44] Yang C-S, Lin M-H, Chang C-H, Yu P, Shieh J-M, Shen C-H, Wada O, Pan C-L. Non-Drude behavior in indium-tin-oxide nanowhiskers and thin films by transmission and reflection THz time-domain spectroscopy. IEEE Journal of Quantum Electronics. 2013;**49**:677-690

[45] Pan C-L, Hsieh C-F, Pan R-P, Tanaka M, Miyamaru F, Tani M, Hangyo M. Control of enhanced THz transmission through metallic hole arrays using nematic liquid crystal. Optics Express. 2005;**13**:3921-3930

[46] Chen C-W, Lin Y-C, Chang C-H, Yu P, Shieh J-M, Pan C-L. Frequency-dependent complex conductivities and dielectric responses of indium tin oxide thin films from the visible to the far-infrared. IEEE Journal of Quantum Electronics. 2010;**46**:1746-1754

[47] Kamoda H, Kuki T, Fujikake H, Nomoto T. Millimeter-wave beam former using liquid crystal. In: Proc. 34th European Microwave Conf., Amsterdam, Netherlands. 2004. pp. 1141-1144

[48] Cheng DK. Field and Wave Electromagnetics. 1st ed. Addison-Wesley; 1983. p. 465

[49] Ku C-P, Shih C-C, Lin C-J, Pan R-P, Pan C-L. THz optical constants of the liquid crystal MDA-00-3461. Molecular Crystals and Liquid Crystals. 2011;**541**:303-308

[50] Kamoda H, Kuki T, Nomoto T. Conductor loss reduction for liquid crystal millimeter-wave beam former. IEICE Electronics Express. 2005;**2**:471-476

[51] Jewell SA, Taphouse TS, Sambles JR. Rapid switching in a dual-frequency hybrid aligned nematic liquid crystal cell. Applied Physics Letters. 2005;**87**:021106

[52] Golovin AB, Shiyanovskii SV, Lavrentovich OD. Fast switching dual-frequency liquid crystal optical retarder, driven by an amplitude and frequency modulated voltage. SID 03 Digest. 2003;**2**(1472):55

[53] Hsieh CT, Huang CY, Lin CH. In-plane switching dual-frequency liquid crystal cell. Optics Express. 2007;**15**:11685-11690

[54] Chen C-C, Chiang W-F, Tsai M-C, Jiang S-A, Chang T-H, Wang S-H, Huang C-Y. Continuously tunable and fast-response terahertz metamaterials using in-plane-switching dual-frequency liquid crystal cells. Optics Letters. 2015;**40**:2021-2024